Precision improvements in ECM via tool insert development by 3D printing

Sneddon, Scott; De Silva, Anjali K.M.; Gomez-Gallegos, Ares A.; Jayasinghe, Prabodha

ISEM XXI

Precision improvements in ECM via tool insert development by 3D printing

Scott Sneddon[1,2], Anjali K.M. De Silva[1*], Ares A. Gomez-Gallegos[1,3], Prabodha Jayasinghe[1]

[1]School of Computing, Engineering and Built Environment, Glasgow Caledonian University, Glasgow, G4 0BA, UK
[2]Precision Tooling Services Ltd, Building 10, Spirit AeroSystems, Prestwick International Airport, Glasgow, KA9 2RW, UK
[3]Department of Mechanical Engineering, Linnaeus University, 351 95, Växjö, Sweden

* Corresponding author Anjali De Silva, School of Computing, Engineering and Built Environment, Glasgow Caledonian University, Glasgow, G4 0BA, UK
Email: ade@gcu.ac.uk

Abstract

This paper reports the tool developments for electrochemical machining (ECM) of precision parts for automotive industry using polymer 3D printed inserts. The role of these inserts is to control the fluid flow in the inter-electrode gap as well as to prevent stray machining by providing insulation. Initial trial and error machining experiments with various tool insert shapes yielded positive outcomes in terms of controlling stray dissolution. It became evident that by 3D printing the entire machining cell structure with integrated, exchangeable tool inserts, all made from polymer, can further enhance the ECM process. This cell-insert assembly enabled better control of the electrochemical dissolution process and allowed for less restrictive flow of the electrolyte, reducing turbulence in the inter-electrode gap. Thus, by improving the electrolyte flow conditions and providing appropriate insulation to prevent stray machining, the 3D printed cell/insert assemblies enabled ECM to achieve a shaped profile of an auto engine component to required tolerances.

Keywords: ECM; 3D printing; Dissolution control.

1. Introduction

Electrochemical machining (ECM) can yield complex geometries in difficult-to-machine metals and theoretically, is capable of achieving dimensional accuracy on the micron level as it removes metal atom by atom by electrolytic dissolution. However, in practice, ECM lacks the dimensional tolerances of comparable processes such as electrical discharge machining (EDM) [1]. The lack of dimensional accuracy is mainly attributed to the superfluous machining that occurs due to stray electric fields. It has been shown by De Silva and Altena [2] that control of electrochemical dissolution and electrolyte flow is critical to achieving precision parts. Due to the stray dissolution control in addition to several other inherent drawbacks including, flow regulation and costs relating to the tool and cell manufacture, ECM finds use only in niche applications. Some of the many efforts to overcome these limitations include non-conductive insulation of the cathode tool to control stray dissolution, open-cell ECM to saturate the work surface with electrolyte, and tool design and electrolyte modelling and simulation. Huang et al. [3] discussed insulating the tool for complex parts is usually difficult time-consuming and inaccurate whilst open-cell methods can incur unwanted turbulent flow characteristics. Advancements in 3D printing technology have shown promising solutions to some of the drawbacks associated with ECM tooling. The work of Lee et al. [4] has shown the use of 3D printing to rapid prototype entire 3D printed cells for electrolytic applications. The 3D

printed cells provide suitable insulation and could be easily optimised to influence flow characteristics. The recent work of Ambrosi et al. [5] has shown that non-conductive 3D printed parts have been utilised for flow and insulation applications such as flow channels, liquid handling components and protective casings.

In this work, ECM is being developed for manufacturing an automotive component of Tribaloy 400 (T400). Currently, the component requires prolonged machining to create profiles that are essential for operation. Machining the component entails a time consuming (single-part) grinding procedure that is manually completed by a machine operator. Aside from the tedious manufacturing time, the process incurs high rates of wear on tools and subsequently increases costs. ECM is considered to reduce manufacturing costs and improve production rates.

This paper highlights the use of polymer 3D printed inserts to control ECM stray dissolution and influence electrolyte flow path. Results from these experiments have led to 3D printing the entire ECM cell and thus, replacing expensive stainless steel machined components with inexpensive 3D printed versions. In addition to reduced manufacturing costs, intricate parts can now be easily created, improving flow control, and hence, machining results.

2. Experimental Approach

2.1. Materials

Tribaloy (T400) workpiece (anode) material was supplied as an ingot and investment cast into single actuator rods at Precision Tooling Services UK, and then machined to size. The cathode tool material is annealed round bar of stainless steel 316, and Wire EDM was used to create the reverse shape profile. The ECM insert and cell were created using SLA 3D printing with a photosensitive clear resin of resin monomer and a photoinitiator. Lastly, a sodium nitrate ($NaNO_3$) electrolyte was used at an initial 10% w/v (i.e. 100 g/l).

2.2. ECM test outline

The requirement is for ECM to remove approx. $108.5mm^3$ of material from T400 actuator rod as shown in Fig. 1. The cross-section image in Fig. 1 (c) highlights the shape change required via ECM to meet the design tolerance of $\pm50\mu m$. A closed-cell design was selected to allow more control over the electrolyte flow and measure key parameters such as flow rate, pressure and temperature entering the cell. Initially, an ECM cell was made from metallic and rubber components to test the 3D printed inserts and determine the optimum insert geometry. The selected insert was then incorporated into a fully 3D printed ECM cell. A selection of tests was conducted with altering parameters such as inter-electrode gap (IEG), flow rate and

conductivity to determine the most suitable parameters for production machining.
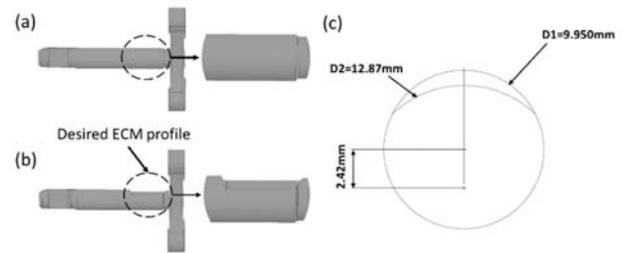
Fig. 1. (a) As-machined T400 actuator rod (b) Required T400 ECM profile (c) Cross-section geometry.

2.3. 3D printing

An Anycubic Mono X SLA 3D printer was used to create a selection of 3D printed inserts (Fig. 2 (a)) to insulate the rod from stray atomic dissolution. A trial and error approach was initially applied to add various radii and undercuts to the 3D printed inserts and their geometrical impact on rod insulation was assessed. A visual representation of the insert and rod assembly are shown in Fig. 2 (b) and (c) with black arrows representing the direction of the electrolyte flow. After each test, the rod was sectioned via wire EDM to analyse each cross-section geometry until the correct shape was found.
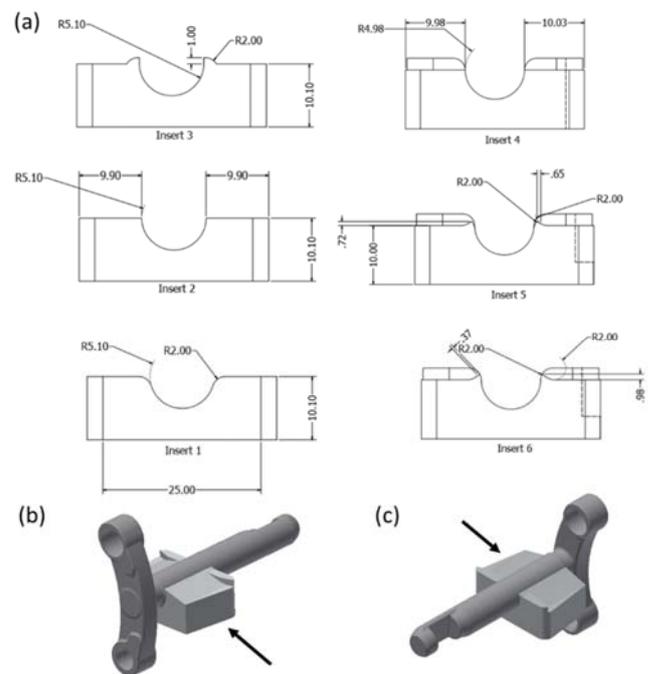
Fig. 2. (a) 3D printed insert insulation variations (b) Insert and rod assembly rear (c) Insert and rod assembly front (black arrow denotes flow direction).

2.4. 3D printed insert tests

The ECM experimental work was conducted on a custom-built structure comprising of a linear z-axis platen displacement method. Stainless steel 316 was chosen as a structural material to provide corrosion protection and rigidity during each test. A Mitsubishi FX5U PLC was used to control the ECM process and a Mitsubishi HGKR73B servo motor equipped with a rotary encoder and electromagnetic braking system controlled the z-axis movement. The servo motor controls a ball screw and stainless steel 316 platen to drive the tool feed. NaO_3 electrolyte was transported into the system at 15-50 Hz with a Grundfos CRI 25 bar pump and filtered through a 1 μm water filter cartridge. A 20V Magna power supply capable of 1000 A' output was employed to power the ECM operation. The temperature was controlled in the clean tank with an RS PRO 9 kW coil heater and a Cosmotec 7KW chiller to cool the spent electrolyte in the dirty tank and maintain a 25°C operating temperature. The electrolyte conductivity was measured before each test with a calibrated Mettler Toledo conductivity measurement probe. A schematic of the insert test is shown in Fig. 3 and the test parameters are listed in Table 2.1.
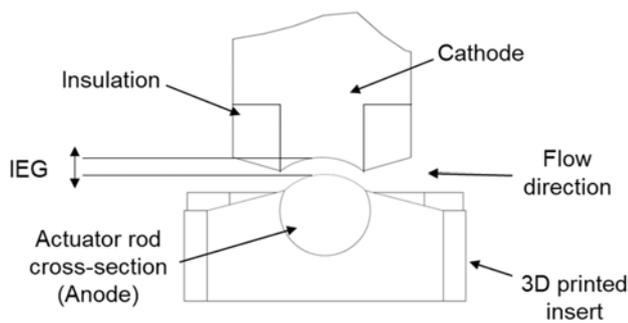
Fig. 3. ECM insert test schematic.

Once the best 3D printed insert was identified, the interelectrode gap (IEG) was reduced periodically until a 75μm gap and 0.75mm/min feed rate was achieved. At this gap size, an unwanted sidestep that previously appeared at the intersection of the rod and insert had been eliminated and repeatable testing was experienced. The flow rate, pressures and temperature were measured in-line for each test. An image of the developed ECM cell used for the insert tests is shown in Fig. 4. The multi-part cell comprises of stainless steel and nylon components. Due to the multiple components, the cell is prone to electrolyte leakage and therefore, a one-part cell is desired.

Table 2.1. Test parameters for ECM insert trials.

Voltage (V)	Current (I)	Current density (J) A/mm²	Electrolyte conductivity (mS/cm)	Flow rate (l/m)	P inlet (bar)
20	70-80	1.6	80.0	7.5	3.0

Fig. 4 – ECM setup for insert trial test.

2.5. Fully 3D printed cell tests

The fully 3D printed cell tests incorporated the most suitable insert from section 2.4. The single-part body was further refined to reduce material wastage. A schematic of the cell is shown in Fig. 5 (a) and a 3D printed version is shown in Fig. 5 (b). A significant reduction in electrolyte leakage was observed during flow trials owing to the reduction of assembled parts and thus, improved flow through the IEG. A variety of tests with different machining parameters were conducted namely; electrolyte conductivity, flow rate and IEG dimensions to obtain the most suitable parameters for production. The tests included in this body of work are outlined in Table 2.2.
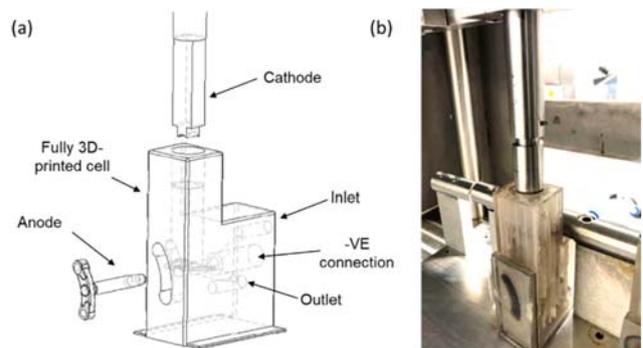
Fig. 5. (a) Full 3D-printed ECM test schematic (b) Full 3D-printed ECM apparatus.

Table 2.2. ECM test outline.

IEG (μm)	125	100	90	80	70	60	55	50
Pump speed (Hz)	15	20	25	30	35	40	45	50
Flow rate (l/m)	3.6	5.4	7.2	8.9	10.5	12	13.7	15.5
Conductivity (mS/cm)	86	96	106	116	-	-	-	-

3. Experimental Results

3.1. Insert trails results

The first set of results to emerge from the study are presented in Fig. 6. Six contrasting inserts were used to insulate the T400 rod from stray current and tested under the test parameters

outlined in Table 2.1. The rods were sectioned via wire EDM and a shadowgraph method was used to highlight variations in shape. The three most significant results are shown to highlight the influence of 3D printed parts on anode insulation. Fig. 6 (a) and (b) display under-machining and over-machining respectively, this is due to inaccurate current control. It can be seen in Fig. 6 (c) that a trial and error method can be used to achieve the correct profile via precise current control. The results from the insert trials show that stray dissolution control plays an important role in achieving the correct shape in ECM. The insert used in Fig. 6 (c) is incorporated into the fully printed ECM cell in section 3.2.
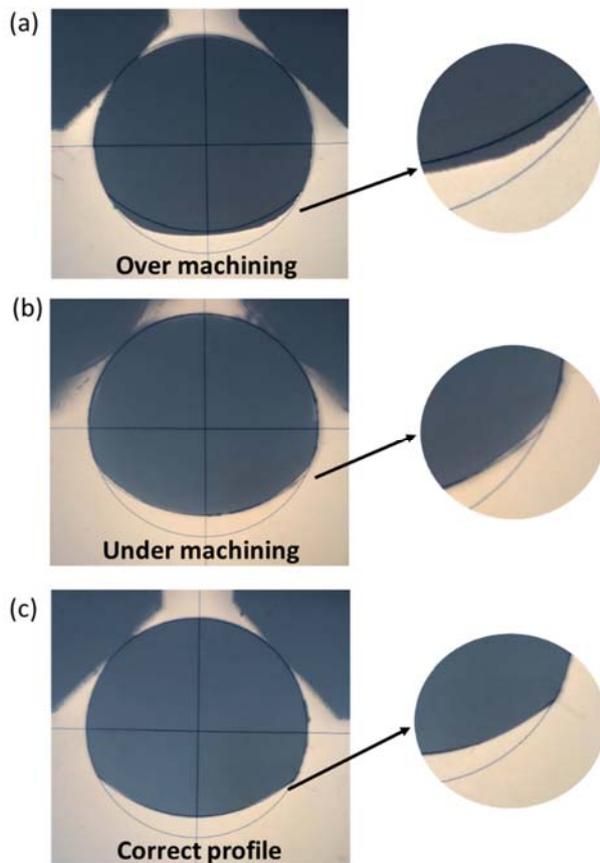
Fig. 6. Shadowgraph of sectioned T400 actuator rods (a) Under-machined (b) Over machined (c) Correct profile.

3.2. Fully 3D printed cell results

The second set of results to emerge from the study are listed in Table 3.1. It can be observed that over machining an increase in initial current is experienced with decreasing IEG towards 50 µm. A smaller IEG localises the electric current at the anode surface, thereby reducing stray dissolution. However, it was shown by Joshi and Marla [6] that small gaps increase the difficulty of electrolyte flushing and increase the chance of electrolyte boiling. The work of Kozak et al. [7] reported that

when using a 10% $NaNO_3$ electrolyte and a steel workpiece, the inter-electrode gap needs to be in the region of 20-50µm for dimensional accuracy and close tolerances in electrochemical micromachining. It was also noted that reduced side and frontal gaps were experienced with increased feed rate. Since pulsed power and reduced voltages are usually utilised in micro-machining, a 50µm IEG was selected as a maximum. This maximum can reduce the likelihood of arcs occurring while maintaining sufficient copying accuracy of the tool.

Table 3.1. Varying IEG test matrix.

Gap (µm)	Flow rate (l/m)	Initial current (A)	Final current (A)	P_{inlet} (bar)	Feed rate (mm/m)	Dimension (mm)
125	9.6	60	73	3.62	0.75	8.96
100	9.3	64	74	3.71	0.75	8.98
90	9.1	65	74	3.75	0.75	8.93
80	9.2	65	73	3.73	0.75	8.93
70	9.0	67	76	3.86	0.8	8.97
60	8.9	75	77	3.80	0.8	8.96
55	8.8	75	81	3.86	0.85	8.97
50	8.9	76	84	3.82	0.85	8.98

The 50 µm IEG was used in determining the effect of electrolyte flow on process variables in ECM. A progressive set of tests were conducted (see Table with a 0.85 mm/m feed rate and an increasing pump frequency from 15-50 Hz at a constant temperature of 25°C. For this set of tests, 20V was applied across the inter-electrode gap. The test was designed to highlight the effect of flow on starting current and final current. This data could then be used to select a suitable flow rate to ensure the initial current and final current did not fluctuate significantly. It is shown in Fig. 7 that flow profiles in the range of 5-9 l/m present uniform current distribution. This is presumed to be due to laminar flow within the IEG. It was discussed by Sawicki and Paczkowski [8] that when the flow velocity is low, the flow profile is laminar in nature however, it was also discussed by Gomez-Gallegos et al. [9] that at reduced flow rates the probability of electrolyte temperature rise and non-uniform machining is increased.
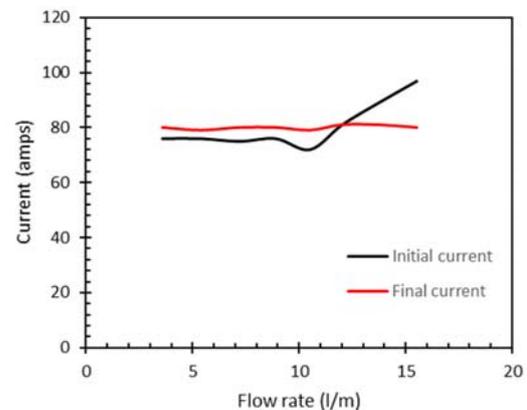
Fig. 7. Flow rate vs current plot.

At high flow rates (>9 l/m), sharp increases in initial current were observed leading to increased temperature and subsequent electrical discharge. This is thought to be due to turbulent flow characteristics in the IEG. Similar findings were observed by Sawicki *et al.* [8] where increased flow rates caused surges in current using a 15% $NaNO_3$ electrolyte and similar parameters.

Table 3.2. Flow rate test matrix.

Test	Pump (Hz)	Flow rate (l/m)	Initial current (A)	Final current (A)	P_{inlet} (bar)	Dimension (mm)
1	15	3.6	76	80	1.88	8.95
2	20	5.4	76	79	2.3	8.97
3	25	7.2	75	80	2.99	8.97
4	30	8.9	76	80	3.82	8.98
5	35	10.5	72	79	4.86	8.99
6	40	12	81	81	6.88	8.94
7	45	13.7	89	81	7.28	8.94
8	50	15.5	97	80	8.67	8.94

The final set of results to emerge from this study are listed in Table 3.3. and plotted in Fig. 8. The conductivity was increased incrementally by adding sodium nitrate to the electrolyte and measuring the conductivity with a probe. For this set of tests, a larger IEG of 75µm was selected due to the increased conductivity and consequent current density. An increase in the average initial current with increasing electrolyte conductivity is observed. The increased machining rate is desirable in certain applications where copying accuracy of anode features is less important such as shape cutting or deburring where non-complex profiles are required. The work of De Silva *et al.* [10] showed that the cathode copying accuracy is greater at low conductivity due to increased localised dissolution. A reduced conductivity can be used to achieve better dimensional control at the expense of machining rate. More so, at reduced conductivity, the probability of sparking is reduced.
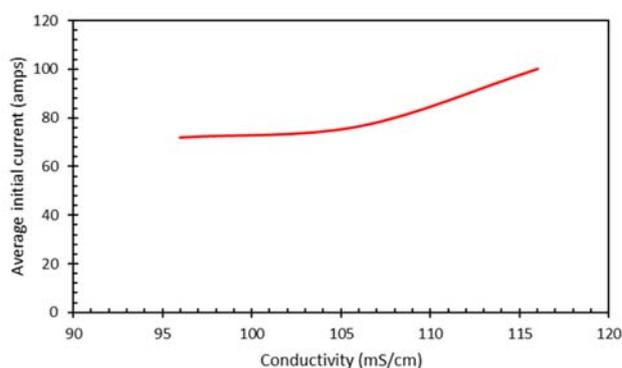
Fig. 8. Conductivity vs average initial current plot.

Table 3.3. Conductivity test matrix.

Conductivity (mS/cm)	Flow rate (l/m)	Initial current (A)	Final current (A)	P_{inlet} (bar)	Dimension (mm)
96	9.2	74	74	3.78	8.91
96	9.3	72	74	3.75	8.92
96	9.3	70	73	3.72	8.94
106	9.0	78	78	3.88	8.88
106	9.2	73	76	3.79	8.88
106	9.3	79	76	3.74	8.88
116	8.6	90	80	4.02	8.76
116	8.5	118	79	3.99	8.78
116	8.5	93	79	4.09	8.79

4. Summary and Outlook

This paper highlights the benefits of using 3D printing polymer parts to aid the tooling developments in ECM so that dissolution and electrolyte flow can be controlled in order to achieve precision. A program of experiments was undertaken to study the influence of 3D printed parts on the dissolution control of an alloy via ECM. A series of insert tests were conducted over a wide range of profiles to promote contrasting dissolution behaviours. After machining, the component profiles were analysed by a shadowgraph method until the desired profile was achieved. The selected insert was incorporated into a fully 3D printed ECM cell where various parameters such as IEG dimensions, electrolyte flow rate and conductivity were investigated. A suitable range of parameters was identified to promote laminar flow, localised dissolution and a resultant dimensional accuracy. An IEG of 50 µm was achieved from an incremental reduction from 125 µm. The 50 µm IEG was used to determine a suitable range of flow rates for production. High surges in current at increased flow rates are due to turbulent flow causing increases in temperature and subsequent current density. An increased machining rate was linked with higher concentrations of $NaNO_3$ electrolyte however, the need for copying accuracy at low concentrations was realised.

Data Availability

- The raw/processed data required to reproduce these findings cannot be shared at this time due to technical or time limitations.

5. References

[1] S. Hinduja and M. Kunieda, "Modelling of ECM and EDM processes", *CIRP Annals - Manufacturing Technology* 62 (2)

[2] A. K. M. De Silva and H. S. J. Altena, "Accuracy Improvements in ECM by Prediction and Control of the Localisation Effects," *International Journal of Electrical Machining,* no. 7, pp. 25-30, 2002.

[3] L. Huang, Y. Cao, C. Tian, R. Zhao, J. Du and Y. Wang, "Study on the Key Technology of Electrochemical Machining Flow Field in Aero-Rotor Blades," *The International Journal of Advanced Manufacturing Technology,* 2021.

[4] L. Huang, Y. Cao, C. Tian, R. Zhao, J. Du and Y. Wang, "Study on the Key Technology of Electrochemical Machining Flow Field in Aero-Rotor Blades," *The International Journal of Advanced Manufacturing Technology,* p. Preprint, 2021.

[5] C.-Y. Lee, A. C. Taylor, A. Nattestad, S. Beirne and G. G. Wallace, "3D Printing for Electrocatalytic Applications," *Joule,* vol. 3, pp. 1835-1849, 2019.

[6] A. Ambrosi, R. R. Sheng Shi and R. D. Webster, "3D-printing for electrolytic processes and electrochemical flow systems," *Journal of Material Chemistry A,* vol. 8, pp. 21902-21929, 2020.

[7] S. S. Joshi and D. Marla, "11.15 - Electrochemical Micromachining," *Comprehensive Materials Processing,* vol. 11, pp. 373-403, 2014.

[8] J. Kozak, K. P. Rajurkar and Y. Makkar, "Selected problems of micro-electrochemical machining," *Journal of Materials Processing Technology,* no. 149, pp. 426-431, 2004.

[9] J. Sawicki and T. Paczkowski, "Effect of the hydrodynamic conditions of electrolyte flow on critical states," in *The European Physical Journal Conferences,* 2015.

[10] A. A. Gomez-Gallegos, F. Mill and A. R. Mount, "Surface finish control by electrochemical polishing in stainless steel 316 pipes," *Journal of Manufacturing Processes,* vol. 23, pp. 83-89, 2016.

[11] A. K. M. De Silva, H. S. J. Altena and J. A. McGeough, "Influence of Electrolyte Concentration on Copying Accuracy of Precision-ECM," in *CIRP Annals,* 2003.